Journal of Power Sources 234 (2013) 119–128

Contents lists available at SciVerse ScienceDirect

Journal of Power Sources

journal homepage: www.elsevier.com/locate/jpowsour

A maximum power point algorithm using the Lagrange method

Sudarshan R. Nelatury*

5101 Jordan Road, School of Engineering, Penn State Erie, Erie, PA 16563-1701, USA

HIGHLIGHTS

- The Lagrange method is employed to find the maximum power point.
- A Seidel type iteration method is used to develop the algorithm.
- Uniqueness of the solution and convergence of the algorithm are mathematically shown.
- A Lagrange maximum power point tracker (LMPPT) is simulated using PSIM and MATLAB.

ARTICLE INFO

Article history:
Received 15 October 2012
Received in revised form
24 January 2013
Accepted 24 January 2013
Available online 1 February 2013

Keywords:
Maximum power point
Lagrange multipliers
Seidel iteration method
Photovoltaic cell

ABSTRACT

The maximum power transfer problem is posed as a constrained optimization problem and the well-known Lagrange method is employed to address it in case of some simple circuits including a photovoltaic cell. In graphical terms, the maximum power point (MPP) is the point of tangency between the isopower contours and the source curve. For the example of a photovoltaic cell a Seidel type iteration is also suggested. A brief mathematical treatment of its convergence and uniqueness of the solution is given along with numerical simulations performed using MATLAB. This new algorithm lends itself to the implementation of the Lagrange MPP tracker (LMPPT). To show its working, the Solarex module MSX-60 is chosen and a simple buck-boost converter circuit is simulated with PSIM software. The terminal current, voltage and power are displayed showing the accuracy and the reliability of the proposed method under varying load and irradiance conditions.

1. Introduction

The maximum power transfer (MPT) theorem is one of the most important theorems in circuits and systems. In the case of a simple dc circuit, it is proved by differentiating the expression for load power, equating to zero and solving for the load resistance, which turns out to be equal to the source resistance. For an ac circuit involving impedances, the load impedance for maximum power equals the conjugate of the source impedance [1]. In both these two situations, the circuit is linear in nature. Of the total power delivered by a linear source, the maximum available to a linear load is 50%. MPT is kept in view wherever it is a concern; as such, circuits, transmission lines and antennas are designed with due consideration to impedance matching. In power systems engineering however, more than MPT, improving efficiency in power distribution is very important. But the growing energy crisis has spawned the pursuit of efficient power generation and delivery and a variety of devices and circuits, several of which are nonlinear, came into the fore. They include photovoltaic (PV) cells produced at industry and consumer scale, space-based solar energy systems, cord-less inductively coupled powering devices, implantable medical devices etc., and many other examples abound. Matching them for efficient energy extraction and tracking the maximum power point (MPP) has now become an intriguing research topic.

The interesting side of MPT is that, it is too simple in the case of a dc circuit but for a linear network of several ports or for a nonlinear circuit, it is indeed too hard. Zhong et al. reported an attempt to trace MPP by an extremum seeking controller in case of fuel cells [2]. Numerous papers appeared in the past two decades proposing ways to identify and track the MPP under varying load/source conditions. For example, [3] provides an interesting review of several algorithms known at the time to identify and track MPP from a PV generator. Exact analytical expression for the MPP in case of nonlinear circuits is known only for some selected cases. Rodriguez and Amaratunga [4] proposed an analytical method that captures the MPP in a small neighborhood.

Most of the MPP tracking schemes are iterative and rule-based in nature. In the recent past, there has been a flurry of activity

* Tel.: +1 814 898 6472; fax: +1 814 898 6125.
E-mail address: srn3@psu.edu.

0378-7753/$ – see front matter © 2013 Elsevier B.V. All rights reserved.
http://dx.doi.org/10.1016/j.jpowsour.2013.01.145

toward the objective of developing fast algorithms to detect and track MPP and the associated hardware to realize them in real time [5–15]. Some of the MPP tracking (MPPT) methods that drew attention were (i) Perturb and Observe method (P&O) (ii) Constant Voltage method (CV), and (iii) Incremental Conductance (IncCond) method. Among these P&O was initially found to be fast but the IncCond suffered from low efficiency and slow convergence. The convergence of CV was reported to be fast but IncCond method was found to exhibit better stability [3,9]. Later, extensive improvements were made to the P&O method by optimizing the parameters of the algorithm. A parabolic prediction in the neighborhood of the MPP was described in Ref. [10] and a distributive MPPT method (DMPPT) was reported in Ref. [11]. The choices of the dc–dc converter topology and parameters, string size and inverter operating voltage have been found to be critical in the design steps of a PV system with DMPPT. An optimal design of a one-cycle controller of a single-stage inverter for PV applications was reported in Ref. [12]. Following this, Femia et al. [13] proposed an optimization technique for a double-stage grid-connected PV system. They have addressed the low-frequency drift problems arising across the bulk capacitor and came up with an analog control network that deals with the duty cycle of the boost converter involved in the controlling power electronics section. Bianconi et al. [14] devised a novel sliding mode control technique for MPP tracking that depends on the current drained by the shunt capacitor across the PV generator. The strength of this method lies in the fast detection of changes in irradiance levels and this new feature was found to be independent of PV array type. More recently, Petrone et al. [15] came up with what they called TEODI approach, which is a distributed scheme and essentially involves an analog circuitry to offset the low-frequency drifts.

In this article, the MPT problem is viewed, in general, as a constrained optimization problem and a graphical picture is presented. The load power expression $V_L I_L = P_L$ represents a family of hyperbolas. Also the load voltage V_L and the load current I_L in case of a simple dc circuit follow a straight line, and in other cases might bear an arbitrary nonlinear relation acting as a constraint. The MPT problem then becomes a constrained optimization problem in terms of the decision variables V_L and I_L to solve which, one could apply the familiar Lagrange method [16]. This approach was earlier adopted by Ahmadi et al. [17] in the context of very large scale photovoltaic power plants. In graphical terms, if the isopower contours and the source line are superimposed, the MPP is the point of tangency. We know that, in general, Lagrange method does not guarantee an optimal solution, but it is *fail-safe* in the sense that, if a solution is found, it must be true. Also the concavity of isopower contours assures a maximum at the point of tangency with the source curve. The overall difficulty of extremizing an objective function depends on the complexity of the source curve and may or may not be easier than the other methods, but the graphical picture offers helpful insights to the circuit designer.

As for the rest of the paper, in Section 2 we shall consider three simple examples: (i) a simple dc circuit, (ii) a diode circuit and (iii) a photovoltaic cell and proceed to find the MPP. The idea behind the first example is to illustrate the method, as standard textbooks such as [1] usually do not employ the Lagrange method. We give an exact expression for the MPP in the case of diode circuit. Thirdly, we address the photovoltaic cell and furnish an approach to obtain the MPP in three easy steps. Section 3 proposes a Seidel type iteration to solve the set of nonlinear equations arising from the Lagrange formulation. This section considers the important questions of existence, convergence and uniqueness that naturally ensue at the outset of such an iteration scheme. The conditions outlined and the possible convergence have been further explained by a simulation example in Section 4.

In order that the proposed method be of any practical utility, one has to devise how it can be implemented in practice. Section 5 details a general schematic for implementation. This configuration bears resemblance with the other existing MPPT systems. The paper subsequently ends in conclusions.

2. The Lagrange method to obtain maximum power

2.1. A simple dc circuit

Consider the simple dc circuit shown in Fig. 1(a) and the relation between V_L and I_L arising from Kirchhoff law shown in (b). In the introduction to diode and transistor circuits, a similar relation has been used and the line represented by it is the familiar load line. We shall call this the *source line* because it has the source resistance term R_S and describes the nature of the Thevenin circuit to the left of the load. In general this line describes how the source voltage E splits between R_S and R_L for a given quiescent current I_Q as indicated in Fig. 1(b). The power expression $V_L I_L = P_L$ may be graphically depicted in the V_L–I_L plane by the contour-plot shown in Fig. 2. The isopower contours are seen to be hyperbolas spreading away from the origin for greater value of power. If a hyperbolic contour corresponding to an arbitrarily small value of power is superimposed on the source line, it intersects at two points shown in Fig. 2 as α and β. But as the contour is gradually moved in search of higher power, α and β coalesce into a single point of tangency and that corresponds to the MPP. Beyond this, there is no intersection

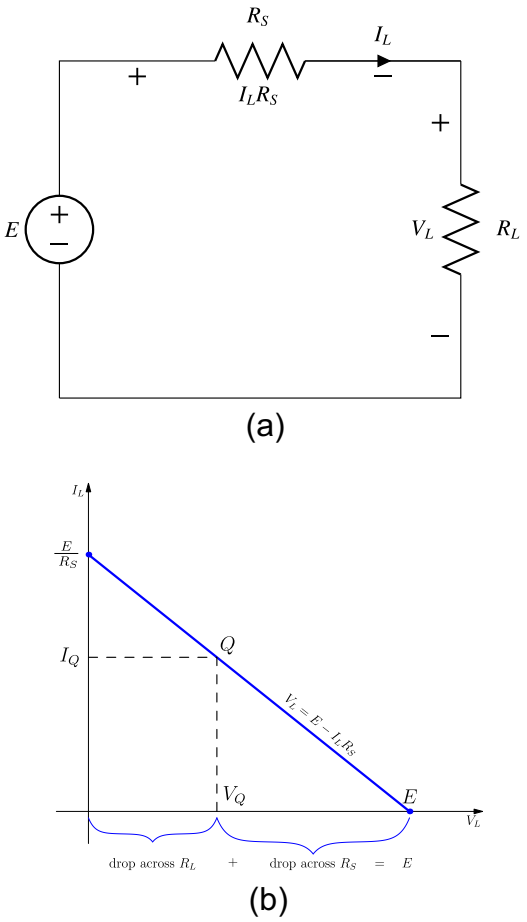

Fig. 1. (a) A simple dc circuit with a source voltage E resistance R_S and load R_L. (b) The relation between V_L and I_L called source line. For a given current I_Q this line shows how E is split between R_S and R_L.

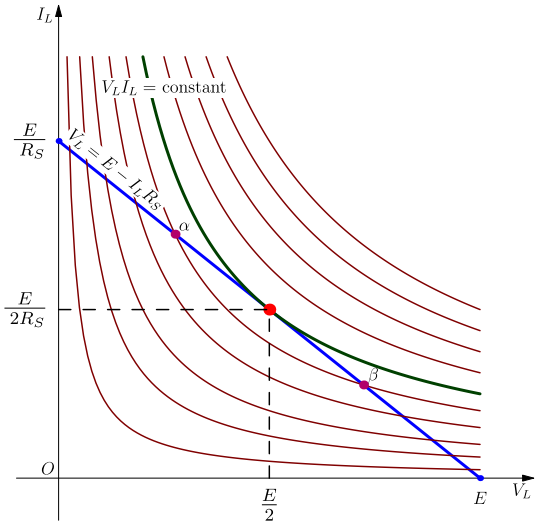

Fig. 2. Isopower contours (brown) and the source line (blue). An arbitrary contour intersects the source line at two points (orange) α and β, which merge into one point shown as ●, where the source line becomes tangential to the maximum power contour (dark green). (For interpretation of the references to colour in this figure legend, the reader is referred to the web version of this article.)

between any of the contours and the source line, implying a non-feasible power in the load. In fact, a quick check shows that solving the two equations (1) and (2) for one of the decision variables, say V_L, yields a quadratic. At the MPP, the discriminant is zero and the single root is the sought-for value of V_L. Considering the power expression as the objective function to be maximized, choosing a Lagrange multiplier λ, let us pose the optimization problem as follows:

$$\text{Maximize}: \; P_L(V_L, I_L) := V_L I_L \tag{1}$$

$$\text{Subject to}: \; S(V_L, I_L) := V_L + I_L R_S - E = 0. \tag{2}$$

From the Lagrange function $\Lambda(V_L, I_L) = P_L(V_L, I_L) + \lambda S(V_L, I_L)$ the optimum is found by solving the system:

$$\frac{\partial \Lambda}{\partial \lambda} = V_L + I_L R_S - E = 0, \tag{3}$$

$$\frac{\partial \Lambda}{\partial V_L} = I_L + \lambda = 0, \tag{4}$$

$$\frac{\partial \Lambda}{\partial I_L} = V_L + \lambda R_S = 0, \tag{5}$$

which yields $V_L = E/2$, $I_L = E/(2R_S)$, $\lambda = -E/(2R_S)$. Since $I_L = E/(R_S + R_L)$, we also get $R_L = R_S$. Not a new result!

2.2. A simple diode circuit

The example in the preceding subsection is too rudimentary and is included just to introduce the idea. Next assume that a pn-diode is included in series with R_S as shown in Fig. 3(a). The current through the diode I_L in terms of the voltage V_D across it are related by $I_L = I_o(e^{\alpha V_D} - 1)$ or equivalently $V_D = 1/\alpha \ln(I_L + I_o/I_o)$, where I_o is the reverse saturation current, $\alpha = q/\eta kT$, q is the magnitude of the electronic charge, k is the Boltzmann constant, T is the absolute temperature and $\eta \approx 1$–2. The source line is now called *source curve*. The optimization problem is updated as below:

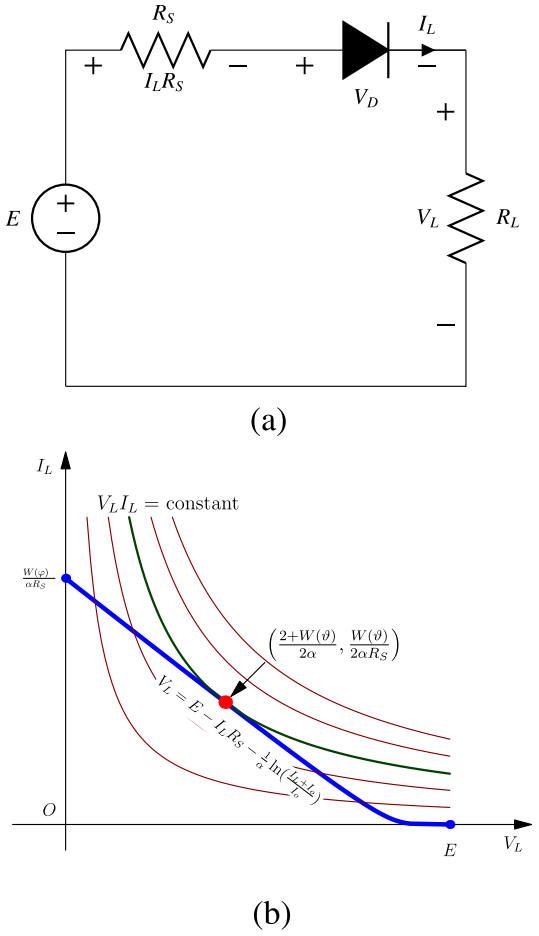

Fig. 3. (a) A simple diode circuit. (b) The source line is tangential to the maximum power contour at the MPP shown in red. (For interpretation of the references to colour in this figure legend, the reader is referred to the web version of this article.)

$$\text{Maximize}: \; P_L(V_L, I_L) := V_L I_L \tag{6}$$

$$\text{Subject to}: S(V_L, I_L) := V_L + I_L R_S + \frac{1}{\alpha}\ln\left(\frac{I_L + I_o}{I_o}\right) - E = 0. \tag{7}$$

The optimum is found by solving the system

$$\left(V_L + I_L R_S + \frac{1}{\alpha}\ln\left(\frac{I_L + I_o}{I_o}\right) - E\right) = 0, \tag{8}$$

$$I_L + \lambda = 0, \tag{9}$$

$$V_L + \lambda\left[R_S + \frac{1}{\alpha(I_L + I_o)}\right] = 0, \tag{10}$$

which is obtained by differentiating the Lagrange function $\Lambda(V_L, I_L) = P_L(V_L, I_L) + \lambda S(V_L, I_L)$with respect to λ, V_L and I_L respectively. From (9) we find that $\lambda = -I_L$, and assuming $I_L + I_o \approx I_L$, we can write $V_L = I_L R_S + 1/\alpha$. This helps us further to modify (8) as

$$2\alpha R_S I_L + \ln\left(\frac{I_L}{I_o}\right) = (\alpha E - 1), \tag{11}$$

which can be simplified as

$$(2\alpha R_S I_L) e^{(2\alpha R_S I_L)} = \frac{2\alpha R_S I_o}{e^{(1-\alpha E)}}. \tag{12}$$

In deriving (12), we make use of the basic properties of logarithms such as $1 = \ln e$, $a \ln e = \ln e^a$ etc. This is a transcendental equation which has a solution in terms of the Lambert-W function [18]. Defining $\vartheta = (2\alpha R_S I_o / e^{(1-\alpha E)})$, we can obtain the MPP as

$$I_L^{\text{opt}} = \frac{W(\vartheta)}{2\alpha R_S}, \tag{13}$$

$$V_L^{\text{opt}} = \frac{2 + W(\vartheta)}{2\alpha}, \tag{14}$$

$$P_L^{\max} = \frac{W(\vartheta)(2 + W(\vartheta))}{4\alpha^2 R_S}. \tag{15}$$

The source curve meets the x-axis at $(E, 0)$ corresponding to an open-circuit load and the y-axis at $(0, W(\varphi)/\alpha R_S)$ where $\varphi = \alpha R_S I_o e^{\alpha E}$ and this corresponds to a short-circuit load. These details are shown in Fig. 3(b). The numerical values used in constructing Fig. 3(b) are given in Table 1 for the sake of clarity. The maximum power with the diode taken into account is 0.2975 W. If the diode is altogether ignored, the maximum power expected would have been $E^2/4R_S = 0.45$ W, a 51.27% overestimation.

2.3. Photovoltaic cell

For more than half a century, photovoltaic (PV) power has been used both on the earth and in space. Unlike some non-renewable sources that cause concern to the atmosphere, solar energy is considered to be harmless and clean. But increasing the efficiency of the PV cells is an important problem being addressed by several researchers. In this example we shall see how we can find the MPP for a typical PV cell. The equivalent circuit of photovoltaic cell that has gained general acceptance [4] is shown in Fig. 4(a). Parallel to the diode there is a current generator whose magnitude I_G depends on the incident radiation. A shunt resistance R_{sh} represents leakage and the series resistance R_{se} characterizes the opposition to electron flow near the contacts and in the overall bulk of the device. The voltage and current at the load terminals are designated by V_{ph} and I_{ph} respectively. We intend to maximize the power $V_{ph}I_{ph}$. The constraint equation comes from the application of the Kirchhoff current law. Thus we pose the problems as:

$$\text{Maximize}: \; P_{ph}\left(V_{ph}, I_{ph}\right) := V_{ph} I_{ph} \tag{16}$$

$$\text{Subject to}: S_{ph}\left(V_{ph}, I_{ph}\right) := I_G - I_o\left(e^{\alpha\left(V_{ph} + R_{se} I_{ph}\right)} - 1\right) - \frac{V_{ph} + R_{se} I_{ph}}{R_{sh}} - I_{ph} = 0. \tag{17}$$

It is easy to note that (17) has the intercept on the x-axis which is the open-circuit voltage given by $V_{OC} = (1/\alpha)\ln[1 + I_G/I_o]$ and

Table 1
Numerical values used in the simulations of Fig. 3.

Parameter	Value	Units
E	3.0	V
α	19.23	V^{-1}
I_o	5	μA
R_S	5	Ω
I_L^{opt}	0.2388	A
V_L^{opt}	1.2459	V
$P_L^{\max}$	0.2975	W
$W(\vartheta)$	45.9185	
$W(\phi)$	46.2188	
$W(\phi)/(\alpha R_S)$	0.4807	A

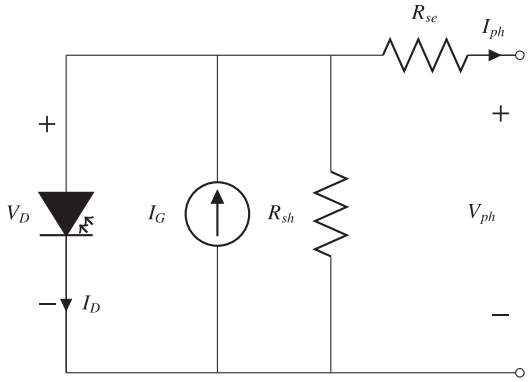

Fig. 4. Equivalent circuit representation of a photovoltaic cell.

likewise the one on the y-axis corresponding to the short-circuit current is given by I_G. Finding partial derivatives of $\Lambda(V_{ph}, I_{ph}) = P_{ph}(V_{ph}, I_{ph}) + \lambda S_{ph}(V_{ph}, I_{ph})$ with respect to λ, V_{ph}, and I_{ph} respectively, the following system of nonlinear equations are obtained:

$$I_G - I_o\left(e^{\alpha\left(V_{ph} + R_{se} I_{ph}\right)} - 1\right) - \frac{V_{ph} + R_{se} I_{ph}}{R_{sh}} - I_{ph} = 0, \tag{18}$$

$$I_{ph} - \lambda\left(\frac{1}{R_{sh}} + \alpha I_o e^{\alpha\left(V_{ph} + R_{se} I_{ph}\right)}\right) = 0, \tag{19}$$

$$V_{ph} - \lambda\left(1 + \frac{R_{se}}{R_{sh}} + I_o R_{se}\alpha e^{\alpha\left(V_{ph} + R_{se} I_{ph}\right)}\right) = 0. \tag{20}$$

The system of equations (18)–(20) is nonlinear and can be solved numerically with a suitable algorithm. Usually, such an algorithm requires an initial guess and one has to ensure its convergence. We propose a very simple approach to obtain a quick solution as follows. In practice R_{se} is small and R_{sh} is very large. First let us assume that $R_{se} \approx 0$ and $R_{sh} \approx \infty$. Equations (18)–(20) can be modified as:

$$I_G - I_o\left(e^{\alpha V_{ph}} - 1\right) - I_{ph} = 0, \tag{21}$$

$$I_{ph} - \lambda\alpha I_o e^{\alpha V_{ph}} = 0, \tag{22}$$

$$V_{ph} - \lambda = 0, \tag{23}$$

which can be analytically solved to get

$$V_{ph}^0 = \frac{1}{\alpha}[W(e(1 + I_G/I_o)) - 1] \tag{24}$$

$$\approx \frac{1}{\alpha} W(e(1 + I_G/I_o)), \tag{25}$$

$$I_{ph}^0 = \alpha I_o V_{ph}^0 e^{\alpha V_{ph}^0}. \tag{26}$$

With the initial values taken from equations (25) and (26), we could iterate

$$I_{ph}^{\ell} = I_G - I_o\left(e^{\alpha\left(V_{ph}^{\ell-1} + R_{se} I_{ph}\right)} - 1\right) - \frac{1}{R_{sh}}\left(I_{ph}^{\ell-1} R_{se} + V_{ph}^{\ell-1}\right), \tag{27}$$

$$V_{ph}^{\ell} = \frac{1}{\alpha}\ln\left[1 + \frac{1}{I_o}\left\{I_G - I_{ph}^{\ell} - \frac{1}{R_{sh}}\left(R_{se} I_{ph}^{\ell} + V_{ph}^{\ell}\right)\right\}\right] - I_{ph}^{\ell} R_{se}. \tag{28}$$

Equations (27) and (28) follow directly from the equivalent circuit shown in Fig. 4 and the equation (17). Let us provide

a numerical simulation to show how MPP is found. For this consider a hypothetical photovoltaic panel consisting of several monocrystalline cells connected in series. The parameter values are close to being typical but here they are assumed as follows. The array is thought of as having 100 monocrystalline cells in series. The simulation study is displayed in Fig. 5. The various values used are given in Table 2. The open-circuit voltage is 60.1458 V, and the short-circuit current is 1.03 A. The initial values obtained from (25) and (26) are 54.8344 V and 2.7998 A respectively. The first two iterations of (27) and (28) are very close the MPP, so their average is considered to be the MPP and is found at $V_{ph}^{\mathrm{OPT}} = 47.9575\,\mathrm{V}$ and $I_{ph}^{\mathrm{OPT}} = 0.9395\,\mathrm{A}$ and $P_{\mathrm{MAX}} = 45.0561$ W. Solving all the three equations (18)–(20) numerically using MATLAB software, we get the optimum for $V_{ph} = 48.1152$ V, $I_{ph} = 0.9539$ A giving the MPP at 45.8971 W.

In order to find the MPP exactly, we need to solve (18)–(20), which are transcendental and whose analytical solution is unlikely. The foregoing discussion has been an attempt to estimate an approximate solution. As for a numerical method to solve the system (18)–(20) that is implementable in real time, we propose an iterative algorithm. The method of iteration is well-known in the field of numerical techniques, but it is expedient that we review the basics briefly and outline the specific steps that lead to actual implementation of an MPP tracker. A key idea in the method of iteration or the so called successive approximation is the contraction mapping principle. These are reviewed in the next section.

3. The method of iteration and contraction mapping

Several numerical approaches are available to solve a system of nonlinear transcendental equations. Not all of them work well for a given situation. An inept choice of method, initial guess, any scale factors used in some of the algorithms might pose the problem of convergence. It is very important that we keep the following in mind while applying an iterative method:

- Existence of solution
- Convergence of the method
- Uniqueness of solution

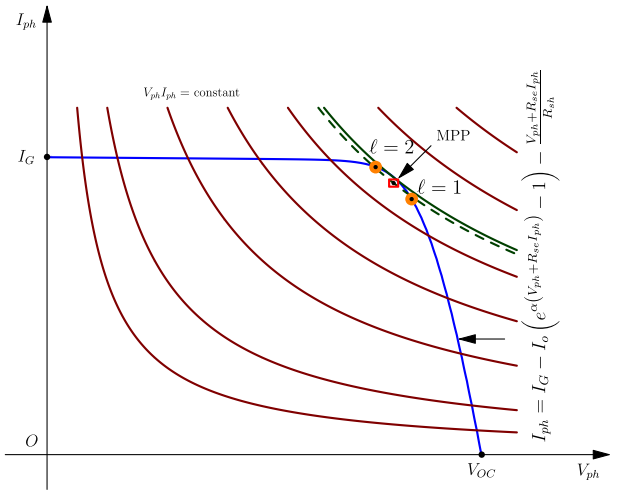

Fig. 5. Finding the MPP in the case of a photovoltaic cell. The first two iterations of (27) and (28) are shown by orange circles. Their average is considered to be the optimum shown in a red box. The MPP is almost closeby. The constant power contour corresponding to this is shown by dark green dashed hyperbola. The contour corresponding to a more accurate value is shown by solid dark green curve. (For interpretation of the references to colour in this figure legend, the reader is referred to the web version of this article.)

Table 2
Numerical values used in the simulations of Fig. 5.

Parameter	Value	Units
I_G	1.03	A
α	0.3868	V^{-1}
I_o	81.1	pA
R_{se}	5	Ω
R_{sh}	5000	Ω
V_{ph}^0	54.8344	V
I_{ph}^0	2.7998	A
V_{ph}^1	50.4505	V
I_{ph}^1	0.8842	A
V_{ph}^2	45.4646	V
I_{ph}^2	0.9948	A
V_{ph}^{OPT}	47.9575	V
I_{ph}^{OPT}	0.9395	A
P_{MAx}	45.0561	W

- Sufficient condition for convergence
- Error estimate in the final solution
- Stopping criterion

Let us address these issues in succession.

3.1. Existence

We can eliminate λ in (18)–(20) and rewrite them as follows:

$$I_{ph} = I_G - I_o\left(e^{\alpha\left(V_{ph}+R_{se}I_{ph}\right)} - 1\right) - \frac{V_{ph}+R_{se}I_{ph}}{R_{sh}}, \tag{29}$$

$$V_{ph} = I_{ph}\frac{\left(1+\dfrac{R_{se}}{R_{sh}}+I_oR_{se}\alpha e^{\alpha\left(V_{ph}+R_{se}I_{ph}\right)}\right)}{\left(\dfrac{1}{R_{sh}}+\alpha I_o e^{\alpha\left(V_{ph}+R_{se}I_{ph}\right)}\right)}. \tag{30}$$

For convenience let us write $I_{ph} = x_1$ and $V_{ph} = x_2$, and use a boldface $\mathbf{x} = [x_1\ x_2]^T$ to represent them as a vector. Likewise, the right hand sides of (29) and (30) are denoted by κ_1 and κ_2 and together, they are indicated by $\boldsymbol{\kappa}(\mathbf{x})$. So we can now combine (29) and (30) as

$$\mathbf{x} = \boldsymbol{\kappa}(\mathbf{x}). \tag{31}$$

Let us assume that the system (29) and (30) has an isolated solution $\mathbf{x}^* = [x_1^*\ x_2^*]^T$ in a neighborhood $D(\mathbf{x}^*, r) = \{\mathbf{y}\in\mathscr{R}^n : \|\mathbf{y}-\mathbf{x}^*\| < r\}$. Where the symbol $\|\cdot\|$ stands for a canonical norm. Further, we note that the functions κ_1 and κ_2 are real, and continuous with bounded partial derivatives in $D(\mathbf{x}^*, r)$. One could approach $\mathbf{x}^*$ by iterating (31) as

$$\mathbf{x}^{\ell} = \boldsymbol{\kappa}\left(\mathbf{x}^{\ell-1}\right) \tag{32}$$

with a starting guess $\mathbf{x}^0$. Suppose the sequence of steps in (32) converge to a value $\boldsymbol{\zeta}$ in the limit

$$\lim_{\ell\to\infty}\mathbf{x}^{\ell} = \boldsymbol{\zeta}, \tag{33}$$

we find

$$\lim_{\ell\to\infty}\mathbf{x}^{\ell} = \lim_{\ell\to\infty}\boldsymbol{\kappa}\left(\mathbf{x}^{\ell-1}\right) \tag{34}$$

which, using *the property of limit of a continuous function* can be written as

$$\lim_{\ell\to\infty}\mathbf{x}^{\ell}=\kappa\left(\lim_{\ell\to\infty}\mathbf{x}^{\ell-1}\right) \tag{35}$$

leading to the conclusion $\zeta=\kappa(\zeta)$ followed by $\mathbf{x}^{*}=\zeta$ and proving the existence of a solution. The limit point $\boldsymbol{\zeta}$ is the *fixed-point* of (31) [19].

3.2. Convergence

In order to ensure the convergence of (31), we shall bring the ideas of (i) contraction mapping in the space $\mathscr{R}^2$ (ii) Cauchy sequence and (iii) closed set.

Let us consider the vectors $\mathbf{x}=[x_1\ x_2]^T\in G\subset\mathscr{R}^2$ and $\mathbf{y}=[y_1\ y_2]^T\in G'\subset\mathscr{R}^2$ related through the mapping

$$\mathbf{y}=\mathbf{f}(\mathbf{x}) \tag{36}$$

defined in the domain $\mathscr{R}^2$. Assume also that $\mathbf{f}$ is Lipschitz continuous in the sense that there exists L, a positive real constant such that $\|\mathbf{f}(\mathbf{x})-\mathbf{f}(\mathbf{y})\|\le L\|\mathbf{x}-\mathbf{y}\|$, $\forall\mathbf{x},\mathbf{y}\in\mathscr{R}^2$. The mapping (36) is called *contraction mapping* in G [19] provided that for $L=\rho$, $0\le\rho<1$, and for any distinct preimages $\mathbf{x}_1$ and $\mathbf{x}_2$, their respective images $\mathbf{y}_1$ and $\mathbf{y}_2$ satisfy

$$\|\mathbf{y}_2-\mathbf{y}_1\|\le\rho\|\mathbf{x}_2-\mathbf{x}_1\|\quad(0\le\rho<1). \tag{37}$$

At this point, although contraction mapping for (31) is an assumption, it will be mathematically proved in a subsequent section. Next, a sequence $\mathbf{x}^0,\mathbf{x}^1,\mathbf{x}^2,\ldots$ is said to be *Cauchy*, if for every positive real number $\varepsilon>0$, however small, there exists $N\in\mathscr{N}$, a positive integer such that $\forall m,n>N$, $\|\mathbf{x}^m-\mathbf{x}^n\|<\varepsilon$. Of course, a *closed set* is one which has all its limit points.

Theorem. Let κ be a contraction mapping in a bounded, convex and closed domain G and let $\mathbf{x}^{\ell}\in$ G at all the successive stages ($\ell=0$, 1, 2,…), then irrespective of the choice of $\mathbf{x}^0$, the iterative process $\mathbf{x}^{\ell}=\kappa(\mathbf{x}^{\ell-1})$ does converge.

Proof. The first step is to prove that the sequence brought into existence through the contraction mapping κ is Cauchy. So let us take two positive integers ℓ,n ($n>\ell$) and consider.

$$\left\|\mathbf{x}^{\ell}-\mathbf{x}^{n}\right\|=\left\|\mathbf{x}^{\ell}-\mathbf{x}^{\ell-1}+\mathbf{x}^{\ell-1}-\mathbf{x}^{\ell-2}+\ldots-\mathbf{x}^{n}\right\|. \tag{38}$$

Using the Minkowski inequality,

$$\left\|\mathbf{x}^{\ell}-\mathbf{x}^{n}\right\|\le\left\|\mathbf{x}^{\ell}-\mathbf{x}^{\ell-1}\right\|+\left\|\mathbf{x}^{\ell-1}-\mathbf{x}^{\ell-2}\right\|+\ldots+\left\|\mathbf{x}^{n-1}-\mathbf{x}^{n}\right\|. \tag{39}$$

By successive application of contraction mapping, it is easy to find that a representative term obeys

$$\left\|\mathbf{x}^{r+1}-\mathbf{x}^{r}\right\|\le\rho^{r}\left\|\mathbf{x}^{1}-\mathbf{x}^{0}\right\|. \tag{40}$$

Hence,

$$\left\|\mathbf{x}^{\ell}-\mathbf{x}^{n}\right\|\le\left\|\mathbf{x}^{1}-\mathbf{x}^{0}\right\|\left(\rho^{\ell-1}+\rho^{\ell-2}+\ldots+\rho^{n}\right) \tag{41}$$

$$\le\left(\frac{\rho^{n}-\rho^{\ell}}{1-\rho}\right)\left\|\mathbf{x}^{1}-\mathbf{x}^{0}\right\| \tag{42}$$

$$\le\left(\frac{\rho^{n}}{1-\rho}\right)\left\|\mathbf{x}^{1}-\mathbf{x}^{0}\right\|. \tag{43}$$

Since $0\le\rho<1$, $\lim_{n\to\infty}\rho^n\to0$, thus, allowing us to conceive of a sufficiently large N, for any $\varepsilon>0$, however small, such that

$$\left\|\mathbf{x}^{\ell}-\mathbf{x}^{n}\right\|<\varepsilon \tag{44}$$

making us to accept that any sequence resulting from the contraction map κ, is Cauchy. However, since G is closed, every limit point is a point of G including every $\boldsymbol{\zeta}$ encountered above. Thus convergence is proved. An important observation is that the convergence is not sensitive to the initial guess. Suffice to say, the subsequent guess belongs to G. In this respect, the iterative process is *self-correcting*.

3.3. Uniqueness

To prove uniqueness, first let us assume that $\mathbf{x}=\kappa(\mathbf{x})$ is true for $\boldsymbol{\zeta}$ and $\boldsymbol{\eta}$ resulting in

$$\boldsymbol{\zeta}=\kappa(\boldsymbol{\zeta}), \tag{45}$$

$$\boldsymbol{\eta}=\kappa(\boldsymbol{\eta}). \tag{46}$$

Subtracting,

$$(\boldsymbol{\zeta}-\boldsymbol{\eta})=\kappa(\boldsymbol{\zeta})-\kappa(\boldsymbol{\eta}). \tag{47}$$

By the Lagrange mean value theorem, there exists $\xi=t\boldsymbol{\zeta}+(1-t)\boldsymbol{\eta}$ for some $0\le t\le1$, that permits us to write

$$(\boldsymbol{\zeta}-\boldsymbol{\eta})=\kappa'(\xi)(\boldsymbol{\zeta}-\boldsymbol{\eta}), \tag{48}$$

$$(\mathbf{I}-\kappa'(\xi))(\boldsymbol{\zeta}-\boldsymbol{\eta})=0 \tag{49}$$

where $\kappa'(\xi)$ is the Jacobian of $\kappa(\mathbf{x})$ evaluated at ξ, $\mathbf{I}=\begin{bmatrix}1&0\\0&1\end{bmatrix}$ and $0=[0\quad0]^T$. Taking the norm $\|\cdot\|_\infty$ on both sides of (49) we get

$$\|\mathbf{I}-\kappa'(\xi)\|_\infty\cdot\|\boldsymbol{\zeta}-\boldsymbol{\eta}\|_\infty=0. \tag{50}$$

The Jacobian of $\mathbf{x}$ is $\mathbf{I}$. The functional expression of κ being transcendental, its Jacobian κ' is not $\mathbf{I}$ over G. This necessitates $\|\boldsymbol{\zeta}-\boldsymbol{\eta}\|=0$ or $\boldsymbol{\zeta}=\boldsymbol{\eta}$, thus proving uniqueness.

3.4. Sufficient condition for convergence

In the foregoing subsections it was proved that convergence and uniqueness are ensured if κ is a contraction mapping. So it remains to elicit a condition that is sufficient to prove that κ affects contraction. From (37) it would suffice if we examine the Lipschitz constant of κ. Toward this end, consider

$$\mathbf{x}-\mathbf{y}=\kappa(\mathbf{x})-\kappa(\mathbf{y}) \tag{51}$$

$$=\kappa'(\mathbf{z})(\mathbf{x}-\mathbf{y}) \tag{52}$$

where $\mathbf{z}=t\mathbf{x}+(1-t)\mathbf{y}$ and $0\le t\le1$. Taking the norm, we get

$$\|\kappa(\mathbf{x})-\kappa(\mathbf{y})\|_\infty=\|\kappa'(\mathbf{z})\|_\infty\cdot\|(\mathbf{x}-\mathbf{y})\|_\infty \tag{53}$$

which reveals that a sufficient condition for κ to be a contraction is

$$\sup_{\mathbf{z}\in G}\|\kappa'(\mathbf{z})\|_\infty\le\rho<1. \tag{54}$$

3.5. Error estimate at the nth iteration

With reference to (33), if the iterative process is carried out *ad infinitum*, we are destined to reach $\boldsymbol{\zeta}$. But if we terminate at the nth iteration, using (43), we can estimate the error accrued in terms of the $\|\cdot\|_\infty$ norm,

$$\|\boldsymbol{\zeta} - \mathbf{x}^n\|_\infty \leq \left(\frac{\rho^n}{1-\rho}\right)\left\|\boldsymbol{\kappa}\left(\mathbf{x}^0\right) - \mathbf{x}^0\right\|_\infty. \tag{55}$$

3.6. Stopping criterion

If an error bound ε is specified, (55) permits us to predetermine the number of iterations required as

$$n = \ln\left[\frac{\varepsilon(1-\rho)}{\left\|\boldsymbol{\kappa}(\mathbf{x}^0) - \mathbf{x}^0\right\|_\infty}\right] \cdot \frac{1}{\ln\rho}. \tag{56}$$

Also from (40), in practice, if the norm of the difference between successive iterates is smaller than a prescribed value, one could terminate the process.

4. Simulation example

4.1. Example continued

In this section we shall repeat the example given in Section 2.3 using the data shown in Table 2. First of all, we need to look into the condition to be met in order that $\boldsymbol{\kappa}$ can be viewed as a contraction. Since that can be done by estimating the Lipschitz number, let us first find the partial derivatives:

$$\frac{\partial\kappa_1}{\partial I_{ph}} = -I_o\alpha R_{se}e^{\alpha\left(V_{ph}+R_{se}I_{ph}\right)} - \frac{R_{se}}{R_{sh}}, \tag{57}$$

$$\frac{\partial\kappa_1}{\partial V_{ph}} = -I_o\alpha e^{\alpha\left(V_{ph}+R_{se}I_{ph}\right)} - \frac{1}{R_{sh}}, \tag{58}$$

$$\frac{\partial\kappa_2}{\partial I_{ph}} = R_{se} + \frac{R_{sh}R_{se}\alpha I_{ph}}{\left(1+I_o\alpha R_{sh}e^{\alpha\left(V_{ph}+R_{se}I_{ph}\right)}\right)^2} + \frac{R_{sh}-R_{sh}R_{se}\alpha I_{ph}}{\left(1+I_o\alpha R_{sh}e^{\alpha\left(V_{ph}+R_{se}I_{ph}\right)}\right)}, \tag{59}$$

$$\frac{\partial\kappa_2}{\partial V_{ph}} = -\frac{I_oR_{sh}^2\alpha^2 I_{ph}e^{\alpha\left(V_{ph}+R_{se}I_{ph}\right)}}{\left(1+I_o\alpha R_{sh}e^{\alpha\left(V_{ph}+R_{se}I_{ph}\right)}\right)^2}. \tag{60}$$

If we numerically calculate each of these four partial derivatives over a domain $0 \leq I_{ph} \leq 1.03, 0 \leq V_{ph} \leq 50$, we find using MATLAB that $|\partial\kappa_1/\partial I_{ph}| + |\partial\kappa_1/\partial V_{ph}| \approx 0.33$ but $|\partial\kappa_2/\partial I_{ph}| + |\partial\kappa_2/\partial V_{ph}| \approx 5488.5$. This shows that κ_1 permits contraction but κ_2 does not. This would cause difficulty for convergence. So to avoid this problem, we propose that the iterative process is carried out in the Seidel way. Instead of iterating $\mathbf{x}^\ell = \boldsymbol{\kappa}(\mathbf{x}^{\ell-1})$, we modify it as $\mathbf{x}_1^\ell = \kappa_1(\mathbf{x}^{\ell-1})$ followed by $x_2^\ell = \kappa_2([x_1^\ell\ x_2^{\ell-1}]^T)$. Our approach is justified because:

(i) The contraction of κ_1 has a built-in self-correcting mechanism as mentioned earlier.
(ii) The expression of κ_2 is free from I_G. Its dependence on irradiation and temperature is reflected in the parameter α and series and shunt resistances. The degree of this dependence is less severe.
(iii) If for a given set of parameters, values of κ_2 are tabulated and consulted, the assumption of closure and boundedness of G is valid.

Numerical simulations reveal that convergence is possible through Seidel iteration thanks to κ_1 alone. Fig. 6 shows κ_1 and the power curve one below the other. Note the MPP in both the curves aligned at the same abscissa. Fig. 7 displays κ_1 and κ_2 on the same graph. Their intersection is the sought-for MPP. We start the Seidel iteration with an initial point on the κ_1 curve at $V_{ph} = 30$ V. Suppose we specify that the final error in I_{ph} for reaching MPP is limited to $\varepsilon = 0.001$. Assuming the overall convergence is controlled by κ_1, we can estimate the number of iterations needed using (56). Substituting $x_1^0 = 1.0229, x_1^1 = 0.9645, \rho = 0.33$ of κ_1, we find $n = \ln[0.001(1-0.33)/(1.0229-0.9645)]\cdot(1/\ln 0.33) = 4.03 \approx 4$. The MPP found by numerically solving (29) and (30) using MATLAB is $V_{ph} = 47.8890, I_{ph} = 0.9613$. We find that the terminal error in I_{ph} is $|0.9613 - 0.9623| = 0.001$. This tallies with our target value. The successive iterations are too crowded in Fig. 7, so they are shown in Fig. 8 at a magnified scale and also furnished in Table 3. The start/stop points, the flow of the algorithm, use of κ_1 and κ_2 maps to get the values along with the arrows in Table 3 illustrate the working of the algorithm.

4.2. Comparison with other methods

To make a quick comparison of the present algorithm with the other existing ones, we shall select [4], in which Rodriguez and Amaratunga discussed an analytical solution to the MPP problem. The first rough approximation for V_{ph} given by them is (See equation (13) in Ref. [4])

$$v_{ph}^* = \frac{1}{\alpha}\ln\left[\frac{I_G}{\alpha I_o(V_{oc} - R_{se}I_G)}\right] - I_GR_{se} \tag{61}$$

which gives a value of 47.0927 V for the data in the present example. They also gave an expression for I_{ph} as (See equation (14) in Ref. [4])

$$i_{ph}^* = I_o + I_G\left(1 - \frac{1}{\alpha(V_{oc} - R_{se}I_G)}\right) \tag{62}$$

which in this case calculates to 0.9816 A. A refinement they have suggested is to resubstitute (62) in equation (12) of [4] is

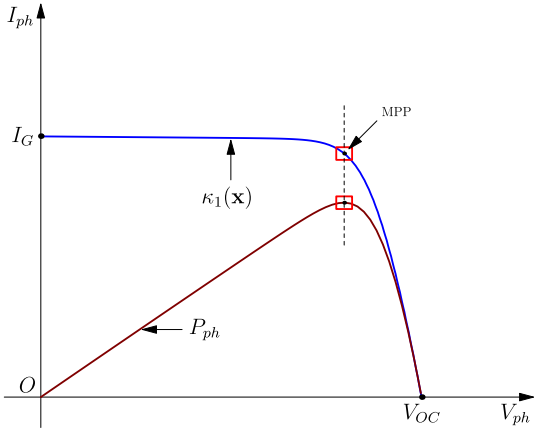

Fig. 6. The MPP shown on $\kappa_1(\mathbf{x})$ and the power P_{ph} curve.

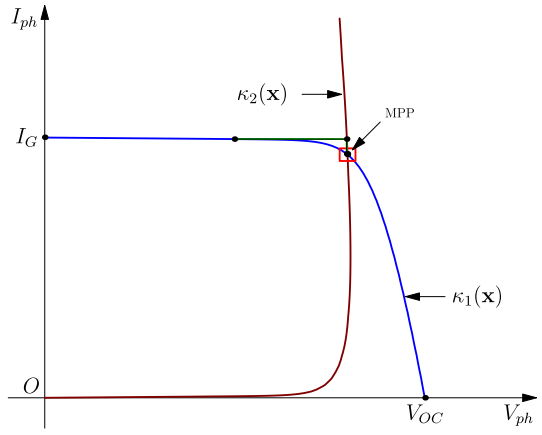

Fig. 7. Intersection of $\kappa_1(\mathbf{x})$ and $\kappa_2(\mathbf{x})$.

$$v_{ph}^{*} = \frac{1}{\alpha}\ln\left[\frac{I_G(R_{sh}+R_{se}-V_{oc}/I_G)}{\alpha I_o R_{sh}(V_{oc}-R_{se}I_G)}\right] - i_{pv}^{*}R_{se}. \tag{63}$$

If we recalculate, this turns out to be 47.3348 V. Since their result is found in one step, we cannot make a fair comparison in every respect. However, in one iteration, the present method has an error in I_{ph} that is 7 times less than theirs and in four iterations the present error in I_{ph} is 20 times less. This single instance may not make the present algorithm superior. Pending actual implementation and testing with real circuitry, however, the underlying Lagrange optimization, coupled with the faster convergence of the Seidel iteration ensure that it could be viewed as an alternative among the various existing techniques.

The formulas given in Section 2.3 permit one to make a quick estimate of the MPP off-line provided all the quantities in (24)–(28) are known a priori. Crucial to this is the knowledge of I_G and the various resistance values. One could get I_G by shorting circuiting the terminals for a few milliseconds. The parameter α depends on the number of cells in the PV panel and the ambient temperature,

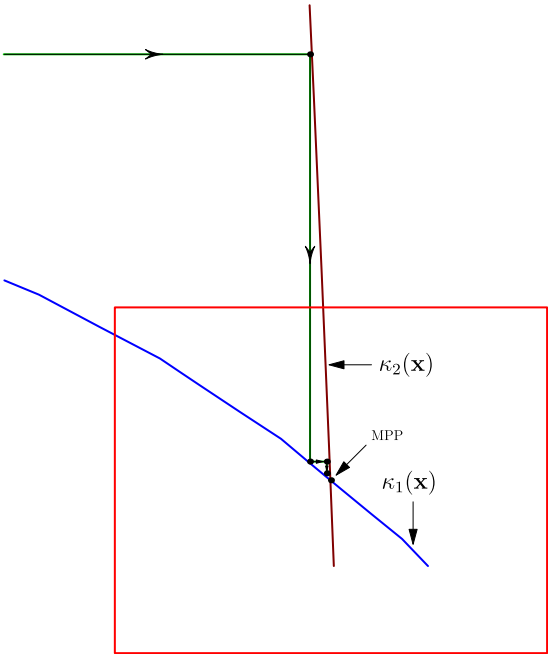

Fig. 8. Successive iterations shown on a magnified scale.

Table 3
Numerical values in the iteration process.

	I_{ph}	1.0229	→ 1.0229	0.9645	→ 0.9645	0.9623	→	Stop
		↑ κ_1		↓ κ_2		↑ κ_1		
Start	→ V_{ph}	→ 30.0000	47.747	→ 47.747	47.8609	→ 47.8609		

which can be measured with the aid of a temperature sensor. With the knowledge of α and I_o, estimation of R_{se} is possible [4]. Or, knowledge of two currents at two smaller voltages helps us to find R_{se}. In dark conditions applying a reverse bias off-line helps us to estimate R_{sh}. These are assumed to be known. The working of LMPPT is based on the two functions κ_1, the device characteristic and κ_2, the latter being independent of I_G; but its values are to be stored in a set of look-up registers. In order to make the discussion more interesting to the experimentalists, in this paper we shall use PSIM software to demonstrate the tracking function.

5. Implementation of the LMPPT

In this section we shall propose a general scheme for implementing the LMPPT. It bears resemblance with the standard configurations found in the references. For example, see Refs. [8] and [4]. Also we shall use PSIM software to perform a circuit simulation and use MATLAB for co-simulating the proposed tracker. In real-life stand alone applications, one is expected to employ voltage and current sensors to read the terminal conditions of the solar panel, a temperature sensor to monitor the temperature, switching circuits to periodically separate the panel and to measure the series and shunt resistances and a micro-controller instead of MATLAB with the necessary data stored in look-up registers for implementation of the LMPPT algorithm.

5.1. Functional description

A load connected to a given PV module receives the maximum power if its resistance equals the optimum value $R_L^{\mathrm{OPT}} = V_{ph}^{\mathrm{OPT}}/I_{ph}^{\mathrm{OPT}}$. If not, the load voltage V_L will be greater than (or less than) V_{ph}^{OPT} depending on whether R_L is greater than (or less than) R_L^{OPT} and the power transferred would be suboptimal. In order to have maximum power transfer, we can insert a DC–DC converter as shown in Fig. 9. The topology for the converter is chosen in relevance to the application at hand. If $R_L < R_L^{\mathrm{OPT}}$, we need to place a buck converter or if $R_L > R_L^{\mathrm{OPT}}$, a boost converter serves the purpose. If the load resistance is expected to vary above and below R_L^{OPT} or if the characteristics of the PV panel vary due to changes in the incident light intensity S or temperature T resulting in such a mismatch, we

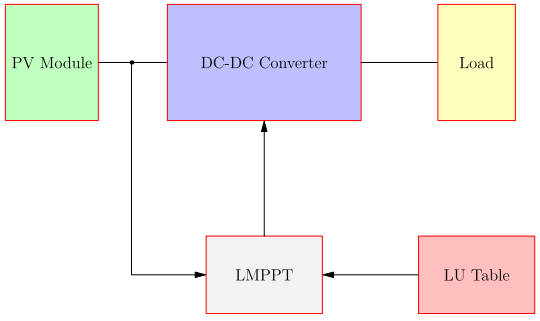

Fig. 9. Block schematic for the Lagrange maximum power point tracker.

can employ a buck-boost converter. Thus the latter is the most suitable for a general application, so an inverting buck-boost topology shown in Fig. 10 is chosen and simulated in this paper. The sampling frequency f_s is conveniently chosen as 100 kHz. The inductor and the capacitor of the converter must be selected based on f_s and the tolerances needed in the load current and voltage respectively. We have judiciously assumed a typical load of 5 Ω and maximum deviation of 10% in the load current I_L and a maximum deviation of 5% in the load voltage V_L and fixed their values in this paper. Also a smoothing low pass filter is prefixed to the converter as shown in Fig. 10 to reduce unwanted oscillations. The optimal MPP coordinates V_{ph}^{OPT} and I_{ph}^{OPT} and the required duty cycle Δ of the converter for optimal power transfer are found via MATLAB. In terms of the load resistance R_L and the MPP coordinates, Δ (expressed in degrees) is estimated using:

$$\Delta = \frac{360 \times \sqrt{I_{ph}^{OPT} R_L}}{\sqrt{I_{ph}^{OPT} R_L} + \sqrt{V_{ph}^{OPT}}}. \tag{64}$$

5.2. PSIM/MATLAB simulation of LMPPT using a buck-boost converter

PSIM is a computer simulation software designed for the analysis and design of power electronics and motor drives. This software has a utility tool called *Solar Module* (*physical model*) that accepts a number of parameters usually listed in the data sheet supplied by the manufacturers. For our simulations, we have selected the MSX-60 of Solarex's Megamodule™ series, made of 36 polycrystalline silicon solar cells. At the standard light intensity of 1000 W m^{-2} and at a temperature of 25 °C, the maximum power obtainable from it is 60 W. We shall first show the maximum power point tracking making four different step changes in the load resistance.

Simulation I: The light intensity and the temperature are assumed to be $S = 1000$ W m^{-2} and $T = 25$ °C respectively. The load resistance is changed with time in four different steps as:

$$R_L = \begin{cases} R_{L1} = 2\Omega & \text{for} \quad 0.0 < t < 2.5\text{ms} \\ R_{L2} = 5\Omega & \text{for} \quad 2.5 < t < 5.0\text{ms} \\ R_{L3} = 6\Omega & \text{for} \quad 5.0 < t < 7.5\text{ms} \\ R_{L4} = 30\Omega & \text{for} \quad 7.5 < t < 10\text{ms} \end{cases} \tag{65}$$

For the present PV module at the given irradiance and temperature values, the series resistance $R_{se} = 8$ mΩ and the shunt resistance $R_{sh} = 1000$ Ω. Also $\alpha \approx 0.8952$. With these parameters, the LMPPT algorithm gives the optimal voltage and current values as 17.14 V and 3.5 A respectively. This permits us to find the duty cycle corresponding to these four different loads as, 140°, 180°, 189°, and 256°. The current, voltage and power at the terminals of the solar panel and at the load terminals are all shown in Fig. 11. As R_L is changed in abrupt steps, note that the PV power P_{ph} in Fig. 11 reached its maximum reasonably fast. For the case of $R_L = 30$ Ω, we do observe some initial fluctuations. This occurs because of the longer time for the under-damped oscillations to settle at this resistance. The power at the output has an average value of approximately 57 W with the remaining 3 W accounted for the losses in the smoothing filter and the buck-boost converter. This reveals the fact that the power transfer efficiency is slightly less than the maximum power point.

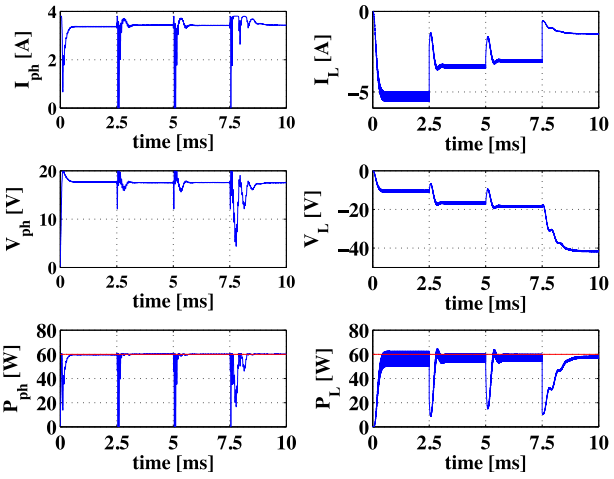

Fig. 11. Showing I_{ph}, V_{ph}, P_{ph}, I_L, V_L, and P_L when load resistance is changed in steps at a constant light intensity of $S = 1000$ W m^{-2} and temperature $T = 25$ °C. The maximum available power of 60 W is shown by a constant line in red. (For interpretation of the references to colour in this figure legend, the reader is referred to the web version of this article.)

Simulation II: Next the load resistance is held constant at 30 Ω and the light intensity is made to fall in steps as:

$$S = \begin{cases} 1000\text{Wm}^{-2} & \text{for} \quad 0.0 < t < 2.5\text{ms} \\ 900\text{Wm}^{-2} & \text{for} \quad 2.5 < t < 5.0\text{ms} \\ 800\text{Wm}^{-2} & \text{for} \quad 5.0 < t < 7.5\text{ms} \\ 700\text{Wm}^{-2} & \text{for} \quad 7.5 < t < 10\text{ms} \\ 600\text{Wm}^{-2} & \text{for} \quad 10 < t < 12.5\text{ms}. \end{cases} \tag{66}$$

The duty cycle in degrees corresponding to these five intensities is found to be respectively, 256°, 252°, 248°, 243° and 237°. As the

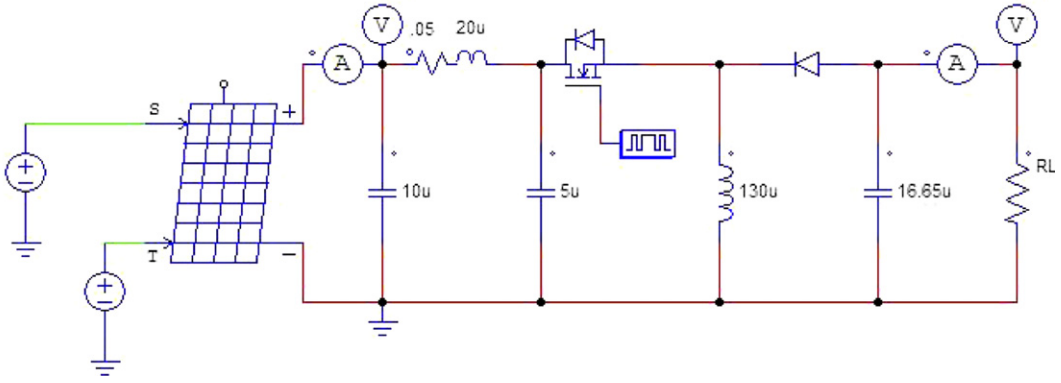

Fig. 10. Buck-boost converter between the solar panel and the load (realized in PSIM).

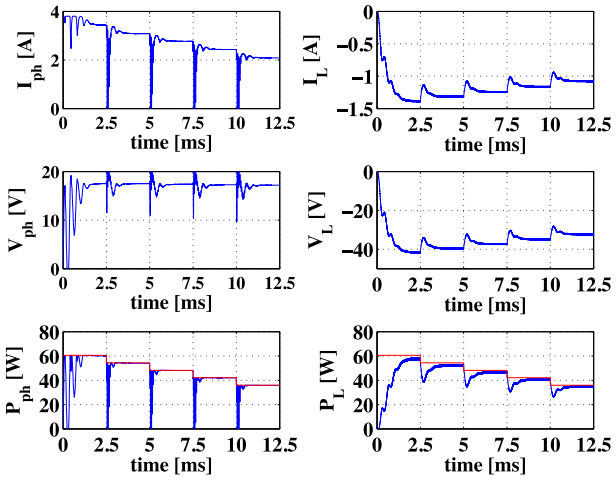

Fig. 12. Showing I_{ph}, V_{ph}, P_{ph}, I_L, V_L, and P_L when the incident light intensity is changed in steps. The load resistance is kept constant at 30 Ω. The maximum available power is shown by a stair-step plot in red. (For interpretation of the references to colour in this figure legend, the reader is referred to the web version of this article.)

light intensity is reduced from 1000 W m^{-2} to 600 W m^{-2}, the available maximum power is reduced from 60 W to about 36 W. Again the current, voltage and the power at the solar panel and at the load terminals are noted and shown in Fig. 12. The results indicate that the MPP tracking is satisfactory.

6. Conclusions

The well-known Lagrange method is used to find the MPP in the case of three simple circuits including a PV cell. For the case of a PV cell, an algorithm based on Seidel iteration is suggested to solve the Lagrange optimization problem. The ideas of convergence and uniqueness are discussed in terms of contraction mapping principle. This algorithm is numerically simulated and found to yield satisfactory results suggesting a possible implementation of LMPPT in real-life applications.

The paper adopted a didactically simpler style to describe the Lagrange method of obtaining the MPP, so that one can apply it even in other similar situations also, where the current I_{ph} is expressed based on other useful models; for example, the multi-exponential model proposed in Ref. [20]. A prototype implementation is shown using PSIM software with the Solarex module MSX-60 and simulations are done to demonstrate the MPP tracking when variations occur in load resistance and also in the intensity of light incident on the solar panel. The convergence of the proposed LMPPT is shown to be reasonably good.

References

[1] C.K. Alexander, M.N.O. Sadiku, Fundamentals of Electric Circuits, fifth ed., McGraw-Hill, 2009.
[2] Z.-D. Zhong, H.-B. Huo, X.-J. Zhu, G.-Y. Cao, Y. Ren, J. Power Sources 176 (2008) 259–269.
[3] V. Salas, E. Olías, A. Barrado, A. Lázaro, Sol. Energy Mat. Sol. Cells 90 (2006) 1555–1578.
[4] C. Rodriguez, G.A.J. Amaratunga, IEEE Trans. Circuits Sys. I: Reg. Pap. 54 (2007) 2054–2060.
[5] O. Wasynezuk, IEEE Trans. Power Appar. Syst. 102 (1983) 3031–3037.
[6] K. Hussein, I. Muta, T. Hoshino, M. Osakada, IEE Proc. Gen. 142 (1995) 59–64.
[7] H.S.H. Chung, K.K. Tse, S.Y. RonHui, C.M. Mok, M.T. Ho, IEEE Trans. Power Electron. 18 (2003) 717–724.
[8] N. Femia, G. Petrone, G. Spagnuolo, M. Vitelli, IEEE Trans. Power Electron. 20 (2005) 963–973.
[9] Y.M. Tung, A.P. Hu, N.K. Nair, Evaluation of Micro Controller Based Maximum Power Point Tracking Methods Using dSPACE Platform, in: Australasian Universities Power Engineering Conference (AUPEC'06) TS-19, Proceedings of the 2006, ISBN: 978 1 86272 669 7.
[10] N. Femia, D. Granozio, G. Petrone, G. Spagnuolo, M. Vitelli, IEEE Trans. Aerosp. Electron. Syst. 43 (2007) 934–950.
[11] N. Femia, G. Lisi, G. Petrone, G. Spagnuolo, M. Vitelli, IEEE Trans. Ind. Electron. 55 (2008) 2610–2621.
[12] M. Fortunato, A. Giustiniani, G. Petrone, G. Spagnuolo, M. Vitelli, IEEE Trans. Ind. Electron. 55 (2008) 2684–2693.
[13] N. Femia, G. Petrone, G. Spagnuolo, M. Vitelli, IEEE Trans. Ind. Electron. 56 (2009) 4473–4482.
[14] E. Bianconi, J. Calvente, R. Giral, E. Mamarelis, G. Petrone, C. Ramos-Paja, G. Spagnuolo, M. Vitelli, A fast current-based MPPT technique employing sliding mode control, in: IEEE International Symposium on Industrial Electronics (ISIE 2011) (2011), pp. 59–64.
[15] G. Petrone, G. Spagnuolo, M. Vitelli, IEEE Trans. Ind. Electron. 59 (2012) 4713–4722.
[16] S.S. Rao, Engineering Optimization Theory and Practice, fourth ed., John Wiley & Sons, 2009.
[17] D. Ahmadi, S.A. Mansouri, J. Wang, Circuit topology study for distribute MPPT in very large scale PV power plants, in: Twenty-sixth IEEE Applied Power Electronics and Exposition (APEC 2011) Proceedings of the 2011 (2011), pp. 786–791.
[18] T.C. Barnwell, A. Jayakumar, Electron. Lett. 36 (2000) 291–292.
[19] W. Rudin, Principles of Mathematical Analysis, third ed., McGrawHill, 1976.
[20] A. Ortiz-Conde, D. Lugo-Muñoz, F.J. García-Sánchez, IEEE J. Photovolt. 2 (2012) 261–268.